

*promoting access to White Rose research papers*



**Universities of Leeds, Sheffield and York**  
**<http://eprints.whiterose.ac.uk/>**

---

This is an author produced version of a paper published in **Journal of Physics: Condensed Matter**.

White Rose Research Online URL for this paper:  
<http://eprints.whiterose.ac.uk/43681>

---

#### **Published paper**

Bryan, M.T., Bance, S., Dean, J., Schrefl, T., Allwood, D.A. (2012) *Transverse and vortex domain wall structure in magnetic nanowires with uniaxial in-plane anisotropy*, Journal of Physics: Condensed Matter, 24 (2), Article no. 024205  
<http://dx.doi.org/10.1088/0953-8984/24/2/024205>

---

# Transverse and vortex domain wall structure in magnetic nanowires with uniaxial in-plane anisotropy

M. T. Bryan<sup>a</sup>, S. Bance<sup>b</sup>, J. Dean<sup>a</sup>, T. Schrefl<sup>b</sup> and D. A. Allwood<sup>a</sup>

<sup>a</sup> Department of Materials Science and Engineering, University of Sheffield, Sheffield S1 3JD, United Kingdom

<sup>b</sup> St. Poelten University of Applied Sciences, St. Poelten, Austria

SHORT TITLE: Nanowires with uniaxial anisotropy

PACS Numbers:

## Abstract

Micromagnetic and analytical models are used to investigate how in-plane uniaxial anisotropy affects transverse and vortex domain walls in nanowires where shape anisotropy dominates. The effect of the uniaxial anisotropy can be interpreted as a modification of the effective wire dimensions. When the anisotropy axis is aligned with the wire axis ( $\theta_a = 0$ ), the wall width is narrower than when no anisotropy is present. Conversely, the wall width increases when the anisotropy axis is perpendicular to the wire axis ( $\theta_a = \pi/2$ ). The anisotropy also affects the nanowire dimensions at which transverse walls become unstable. This phase boundary shifts to larger widths or thicknesses when  $\theta_a = 0$ , but smaller widths or thicknesses when  $\theta_a = \pi/2$ .

## 1. Introduction

For many years, Permalloy ( $\text{Ni}_{81}\text{Fe}_{19}$ ) has been the material of choice for investigations of patterned magnetic elements, as it possesses negligible magneto-crystalline anisotropy and magnetostriction. This means that the shape of the element can be used to control many magnetic properties, from the local magnetisation direction [1,2] to domain wall nucleation [3-5] pinning [6-10] and propagation characteristics [11-13]. In addition, the shape can also govern the type of domain wall that can form, as head-to-head (or tail-to-tail) domain walls tend to form in nanowires. Depending on the wire width and thickness, the head-to-head wall may have a 'transverse' structure, characterised by a purely in-plane magnetization rotation, or form a vortex configuration, characterised by a circulation of magnetisation around a central core oriented out-of-plane [14,15]. The different magnetisation configurations within transverse and vortex walls lead to differences in propagation and pinning behaviour [16] which could affect the reliability of nanowire devices.

Recent investigations have explored using materials that exhibit magneto-crystalline anisotropy [17-19] or stress-induced anisotropy [20-22], in addition to the shape anisotropy. Much of this work is driven by interest in multiferroic systems, which exhibit changes in anisotropy in response to an electric field. Provided they do not dominate the energy landscape [23], such "additional" in-plane anisotropies could be used to reinforce the effect of the shape anisotropy in a nanowire, which could stabilize magnetization as dimensions approach the superparamagnetic limit. In-plane anisotropy can also allow control over the velocity and Walker breakdown fields of domain walls [21]. Recent modelling has shown how localized changes in the anisotropy of an artificial multiferroic device, formed from a magnetostrictive nanowire coupled to a piezoelectric material, could allow low power

positioning of domain walls [22], providing a switchable functionality not possible with shape anisotropy alone.

Here, we describe how micromagnetic and analytical models are used to examine the effect of an additional in-plane uniaxial anisotropy on domain wall width and the phase boundary between transverse and vortex walls. We discuss the effect in general terms, so the in-plane anisotropy could be magnetocrystalline or magnetostrictive in origin.

## 2. Finite element modelling

A finite element micromagnetic model [24,25] was used to solve the Landau-Lifshitz-Gilbert equation for smooth-sided wires containing either a vortex or a transverse domain wall. The wires studied were 50-300 nm wide and 5-20 nm thick, with a constant aspect ratio (length-to-width ratio) of 15 to minimise interactions between the wall and the wire ends. Wedge-shaped wire ends, inclined at  $45^\circ$  to the wire long axis (the x-axis, Fig. 1), were used to ensure all simulations had a similar end domain structure. To examine the effect of an in-plane anisotropy on the domain wall structure, the wire was modelled with magnetic properties similar to Permalloy (exchange stiffness constant,  $A = 10 \text{ pJ.m}^{-1}$ ; saturation magnetisation,  $M_s = 800 \text{ kA.m}^{-1}$ ), but with an additional in-plane anisotropy,  $K$ , with an easy axis directed at an angle  $\theta_a$  to the wire long axis (Fig. 1). In order to ensure that the dominant anisotropy was due to shape, the maximum value of  $K$  was restricted to  $10 \text{ kJ.m}^{-3}$  [21]. As only the static wall structure was needed, the Gilbert damping constant was set to  $\alpha = 1$  to allow rapid convergence in calculations.

Figure 1 shows axial magnetisation profiles ( $M_x/M_s$ ) calculated by finite element modelling, taken along the centre of the wire, of transverse and vortex walls in a 150 nm wide, 10 nm

thick wire when  $K = 0 \text{ J.m}^{-3}$  and  $K = 10 \text{ kJ.m}^{-3}$  for  $\theta_a = 0 \text{ rad}$  and  $\theta_a = \pi/2 \text{ rad}$ . The profiles show that while  $M_x$  changes approximately linearly across the width of transverse walls when  $K = 0 \text{ J.m}^{-3}$  or  $\theta_a = 0 \text{ rad}$  (Figs. 1a and 1b), deviations from this linearity occur when  $\theta_a = \pi/2 \text{ rad}$  (Fig. 1c). On the other hand, a highly non-linear variation of  $M_x$  is seen across all the vortex walls, particularly around the vortex core. The calculated wall structures show that the magnetisation profile changes across the wire width, leading to a difficulty in defining a unique domain wall size. For the micromagnetic model, we define the wall boundaries as the points along the centre of the wire where  $M_x/M_s = \pm 0.9$ . This definition allows transverse and vortex walls to be compared without assuming a particular form to the magnetisation profile. Without an in-plane anisotropy, the vortex wall has a width of  $w_{VW} = 258 \text{ nm}$ , while the transverse wall has a width of  $w_{TW} = 124 \text{ nm}$ . Under an in-plane anisotropy with easy axis parallel to the wire long axis (Fig. 1b), the wall widths decrease to  $w_{VW} = 218 \text{ nm}$  and  $w_{TW} = 101 \text{ nm}$ . The reduction is due to the in-plane anisotropy reinforcing the shape anisotropy in the wire. Correspondingly, when the in-plane easy axis is perpendicular to the wire long axis, the in-plane anisotropy acts against the shape anisotropy, increasing the wall width ( $w_{VW} = 324 \text{ nm}$  and  $w_{TW} = 163 \text{ nm}$ ) above the width that occurs without an in-plane anisotropy. In each case, the vortex wall width is roughly twice that of the transverse wall.

### **3. 1D analytical modelling**

#### *3.1 Wall width*

The changes in the wall width with anisotropy direction are consistent with the concept that the superposition of the in-plane and shape anisotropies acts to change the effective wire dimensions [21]. To examine this in more detail, the in-plane anisotropy was included in a

one-dimensional (1D) analytical model. Analytically, the structure of a transverse wall can be defined as  $\cos(qz)$ , where  $q$  is the distance from the wall centre and  $\Delta_{TW}$  is the wall width parameter [26]. The micromagnetic model shows that the magnetisation in the domain walls varies across two dimensions (Fig. 1). Nevertheless, the 1D analytical model agrees with the micromagnetic profile across the narrowest part of the transverse wall (the bottom edge of the transverse walls shown in Fig. 1), so it can provide a useful platform to analyse changes in the wall structure. The wall width parameter of a transverse wall under an in-plane anisotropy  $K$  with easy axis  $\theta_a$  to the wire long axis (x-axis) is given by

$$\Delta_{TW} = \frac{\mu_0 M_s}{\sqrt{K - \mu_0 N_y \sin^2 \theta_a - \mu_0 N_z \cos^2 \theta_a}}$$

where  $\varphi$  describes the out-of-plane (azimuthal) rotation angle of the wall ( $\varphi = \pi/2$  rad for a stationary wall),  $\mu_0$  is the permeability of free space, and  $N_y$  and  $N_z$  are demagnetisation factors in the transverse (y-) and out-of-plane (z-) directions, which can be calculated from the ratio of the wire width and thickness [12]. Equation 1 predicts transverse domain wall widths ( $\pi\Delta_{TW}$ ) of 52 nm, 46 nm and 62 nm for the cases of  $K = 0 \text{ J.m}^{-3}$  and  $K = 10 \text{ kJ.m}^{-3}$  for  $\theta_a = 0$  rad and  $\theta_a = \pi/2$  rad in a wire identical to that shown in fig. 1. In each case, the analytical wall width is approximately 40% of the corresponding micromagnetically calculated wall width, due to the different definitions of wall width. The effect of the wall width definition can largely be removed by normalizing the wall widths to the case without anisotropy. The structure of vortex walls is clearly more complicated than transverse walls (Fig. 1). However, noting that a vortex wall consists of two halves similar to two opposing transverse walls, we approximate the vortex wall width to  $\Delta_{VW} \approx 2\Delta_{TW}$ . This is similar to the

wall width ratio derived elsewhere [15] and is consistent with the values calculated micromagnetically from Fig. 1.

Comparing Eq. 1 with the wall width parameter obtained when  $K = 0 \text{ kJ.m}^{-3}$ , the effect of the in-plane anisotropy can be described in terms of “effective” demagnetisation factors, and  $\Delta_{TW}$ , that include the uniaxial anisotropy, so that

$$\frac{\Delta_{TW}}{w/t} = \frac{N_{eff}}{w/t} \quad (3)$$

For  $180^\circ$  walls, these terms replace the actual demagnetisation factors used in analytical models that neglected uniaxial anisotropy. Thus the effect of the uniaxial anisotropy can be intuitively understood in terms of altering the effective width,  $w'$ , and thickness,  $t'$ , of the wire, assuming that the relationship between the effective wire dimensions and demagnetisation factors is identical to the case without uniaxial anisotropy [12]:

$$\frac{w'}{t'} = \frac{w}{t} \quad (4)$$

$$(5)$$

To illustrate this, fig. 2a shows the effective dimensions determining  $\Delta_{TW}$  when the wall is stationary (i.e. the  $w'/t'$  that satisfy Eq. 4) for a wire with a physical width-to-thickness ratio of  $w/t = 20$  under various anisotropy conditions. When  $\theta_a = 0 \text{ rad}$ , the effective  $w/t$  experienced by  $\Delta_{TW}$  is actually smaller than the physical width-to-thickness ratio. As the anisotropy angle increases, the effective width-to-thickness ratio of the stationary wall width also increases, such that for  $\theta_a > \pi/4 \text{ rad}$   $\Delta_{TW}$  is determined by an effective  $w/t$  larger

than the physical width-to-thickness ratio. These results are consistent with the micromagnetic model (fig. 1), which show that when  $\theta_a = 0$  rad, the wall width is smaller than the case with no anisotropy, while when  $\theta_a = \pi/2$  rad, the wall width is enhanced. In addition to the increase in  $\Delta_{TW}$ , the Walker breakdown field,  $H_w$ , also increases with  $\theta_a$  (fig. 2b), in qualitatively similar behaviour to that observed in previous micromagnetic models below  $\pi/3$  rad ( $60^\circ$ ) [21]. That  $H_w$  is independent of  $K$  when  $\theta_a = 0$  rad may be indicative of the different dependence of the Walker breakdown field and wall width on the wire dimensions [13].

Figure 3 shows a comparison between the analytical and micromagnetic wall widths (using  $\varphi = \pi/2$  rad) when  $K = 10 \text{ kJ.m}^{-3}$ , normalised to the case where  $K = 0 \text{ kJ.m}^{-3}$ . The analytical model predicts the general form of the  $\theta_a$  dependence for the vortex wall, except that the micromagnetic data have an additional phase shift of around  $\pi/12$  rad ( $15^\circ$ ) for clockwise walls and  $-\pi/12$  rad for counter-clockwise walls. The chirality-dependence of the vortex wall width is caused by rotational asymmetry within the vortex wall structure, which is reinforced in clockwise walls when  $\theta_a > 0$  rad and in counter-clockwise walls when  $\theta_a < 0$  rad. The polarity of the vortex cores, while not explicitly studied here, is not expected to influence the effect of the anisotropy on the wall width. In contrast to the chiral effects seen in vortex walls, transverse walls with magnetisation parallel to the positive or negative  $y$ -directions behave identically. Transverse walls follow the same trend as clockwise vortex walls when  $\theta_a > 0$ , but when  $\theta_a < 0$  they follow the same trend as counter-clockwise vortex walls. It is likely that asymmetry in the wall structure, such as that seen in Fig. 1c, may be responsible for the observed dependence of the transverse wall width. Despite not accounting for the wall asymmetry, the 1D analytical model does reproduce the underlying

form of the micromagnetic data, suggesting that it contains most of the terms needed to understand the system. Significantly, all walls have similar normalised widths when the in-plane anisotropy axis lies either parallel ( $\theta_a = 0$  rad) or perpendicular ( $\theta_a = \pi/2$  rad) to the wire. This is precisely what is expected from the 1D analytical model, suggesting that when the in-plane anisotropy axis lies along a symmetry axis of the wire, the effect of the wall asymmetry on the wall width is negligible.

### 3.2 Wall structure

In addition to changing the domain wall width, the in-plane anisotropy also alters the domain wall energy. As vortex and transverse walls have different magnetisation structures, they have different responses to the in-plane anisotropy. We used finite element modelling to determine the wire dimensions at which transverse walls have lower energy than vortex walls, defining a phase boundary of wall type stability. Points on this boundary are shown in Fig. 4 for  $K = 0 \text{ J.m}^{-3}$ , and  $K = 10 \text{ kJ.m}^{-3}$  with  $\theta_a = 0$  rad and  $\theta_a = \pi/2$  rad. The  $K = 0 \text{ J.m}^{-3}$  case follows previous phase boundary calculations [14,15]. We neglect the phase boundary between symmetric and asymmetric transverse walls [15], although we note that this boundary is also affected by the in-plane anisotropy, as indicated by the wall structures shown in Figs. 1a and 1b. Figure 4 shows that when the easy axis of the in-plane anisotropy is parallel to the wire long axis ( $\theta_a = 0$  rad), the vortex/transverse phase boundary shifts so that for a given thickness, wider wires can support transverse walls. This is consistent with a decrease in effective wire width, as the phase boundary behaves as if the wires are narrower than they really are. On the other hand, when  $\theta_a = \pi/2$  rad, the phase boundary is shifted to narrower widths (the effective wire width increases), allowing wires with small cross-sectional dimensions (width 165 nm, thickness 5 nm) to support stable vortex walls.

This means that the introduction of a uniaxial in-plane anisotropy, for example via a forming field during deposition [27], could change the stable configuration of a domain wall in a magnetic nanowire. A switchable uniaxial anisotropy, such as by the piezoelectric actuation of a magnetostrictive wire [22], could lead to the selective destabilisation of one type of wall structure in favour of the other. Transformation to a lower energy wall state may require thermal activation to overcome the energy barrier between the wall types [28]. While beyond the scope of this study, it is also possible that uniaxial anisotropy could directly influence the energy barrier between transverse and vortex states, given that the direction of anisotropy can determine whether a transverse wall undergoes Walker breakdown via a transition to an anti-vortex state or a vortex state [21].

The shift in the phase boundary can be understood by considering the conditions under which there is no energy difference between vortex and transverse walls. Analytical descriptions of the exchange and demagnetisation energy differences,  $E_{ex}$  and  $E_{dm}$ , were deduced in previous work neglecting in-plane anisotropy [14] ( $r_{max}$  and  $r_{core}$  are the outer and core radii of the vortex).

The in-plane anisotropy energy,  $E_{in}$ , for transverse wall is given by

for  $\varphi = \pi/2$  rad, where  $w$  and  $t$  are the wire width and thickness, respectively. The in-plane anisotropy energy,  $E_{in}$ , for vortex walls has a similar form, but with an additional term describing the vortex core. As we approximate the wall width parameter of vortex walls to  $2\Delta_{TW}$ , the energy difference between vortex and transverse walls is given by

Minimizing the total energy ( $\Delta E_{\text{ex}} + \Delta E_{\text{ms}} + \Delta E_{\text{ani}} = 0$ ), we can determine the relation between the wire width,  $w_b$ , and thickness,  $t_b$ , at the vortex/transverse wall phase boundary:

$$\frac{w_b}{t_b} = \frac{K}{\mu_0 M_s^2} \left( \frac{1}{\sin^2 \theta_a} - 1 \right)$$

The vortex core radius is on the scale of the exchange length, so we assume  $r_{\text{core}} \approx 5$  nm. Here, we find that  $r_{\text{max}}/r_{\text{core}} = 8$  gives a good fit to the micromagnetic model when  $K = 0$  kJ.m<sup>-3</sup> (Fig. 4). The analytical solutions agree reasonably well with the micromagnetic model when  $\theta_a = \pi/2$  rad with  $K = 10$  kJ.m<sup>-3</sup> but tend to overestimate the effect of the in-plane anisotropy when  $\theta_a = 0$  rad (fig. 4). Further analysis of Eq. 8 reveals that the anisotropy energy due to the vortex core contributes relatively little to the shift in the phase boundary. More significant is the relative difference between the widths of the transverse and vortex walls. When  $\theta_a = \pi/2$  rad, the anisotropy energy decreases with a greater degree of magnetisation across the wire width, so the larger width of vortex walls is advantageous and the phase boundary is shifted to lower wire widths. On the other hand, when  $\theta_a = 0$  rad, the anisotropy energy is minimised when the axial domain magnetisation is maximised, favouring the smaller width of transverse walls and shifting the phase boundary to higher wire widths. However, the 2D structure of the vortex wall means that some magnetisation components in the wall will still be aligned with the in-plane anisotropy axis when  $\theta_a = 0$  rad, reducing the overall energy of the wall. This explains why the analytical model overestimates the effect of the in-plane anisotropy on the phase boundary when  $\theta_a = 0$  rad.

The structure of a head-to-head domain wall has a large effect on its dynamic behaviour. Field-dependent and spin-polarised current-dependent domain wall mobilities differ for

transverse and vortex walls, with transverse walls generally travelling faster [15, 29-31]. The type of domain wall also affects strongly interactions with deliberate defects in wire edges, which are often used to control domain wall position, and very different de-pinning fields can be observed with the two wall types [16]. Reliable device operation will usually require domain wall structure to be preserved. A uniaxial anisotropy could also be useful in preventing Walker breakdown and the accompanying oscillations in magnetisation configuration [11, 21, 32].

#### **4. Summary**

The structure of transverse and vortex domain walls in nanowires with in-plane anisotropy was investigated using micromagnetic and analytical models. The transverse and vortex wall widths depend on the strength of the anisotropy and the angle of the in-plane easy axis with respect to the wire easy axis,  $\theta_a$ . In addition, the vortex wall width was dependent on the vortex chirality, except when  $\theta_a = 0$  rad and  $\theta_a = \pi/2$  rad. At every  $\theta_a$ , the largest vortex walls were approximately twice as wide as the transverse walls. Narrower walls occur when the in-plane easy axis is aligned with the wire long axis ( $\theta_a = 0$  rad), whereas wider walls occur when the in-plane easy axis is perpendicular to the wire axis ( $\theta_a = \pi/2$  rad). Conceptually, this can be understood in terms of the in-plane anisotropy altering the effective wire dimensions experienced by the wall width, so that for a given thickness, the wire behaves as if it is narrower than it actually is when  $\theta_a = 0$  rad, but wider  $\theta_a = \pi/2$  rad. Analytical models accounting for the change in the effective wire dimensions reproduced a similar response of the Walker breakdown field to the anisotropy as is seen in micromagnetic models. This suggests that the effect of uniaxial anisotropy on other

dynamic quantities, such as the wall velocity or the de-pinning field from a defect, may also be understood in terms of modifying the effective wire dimensions.

The change in effective wire dimensions alters the phase boundary describing the stability of transverse and vortex walls in the nanowire, such that the phase boundary is shifted to larger widths or thicknesses when  $\theta_a = 0$  rad, but smaller widths or thicknesses when  $\theta_a = \pi/2$  rad. The main contribution to the shift in the phase diagram is the difference between the transverse and vortex wall widths. Given the recent interest in fabricating nanostructures from materials with magnetocrystalline anisotropy and the emerging field of piezoelectric-controlled magnetic anisotropy with artificial multiferroic structures, knowledge of how the phase boundary shifts in the presence of in-plane anisotropy could benefit both fundamental studies and future technologies.

### **Acknowledgements**

We would like to thank EPSRC for their financial support under grant numbers EP/F069359/1 and EP/G032300/1.

### **References**

- [1] O'Shea K J, McVitie S, Chapman J N, and Weaver J M R 2008 *Appl. Phys. Lett.* **93** 202505
- [2] Bryan M T, Smith K H, Real M E, Bashir M A, Fry P W, Fischer P, Im M Y, Schrefl T, Allwood D A, and Haycock J W 2010 *IEEE Magn. Lett.* **1** 1500104
- [3] Kirk K J, Chapman J N, and Wilkinson C D W 1999 *J. Appl. Phys.* **85** 5237
- [4] Yi G, Aitchison P R, Doyle W D, Chapman J N, and Wilkinson C D W 2002 *J. Appl. Phys.* **92** 6087

- [5] Bryan M T, Atkinson D, and Cowburn R P 2005 *J. Phys: Conf. Seri.* **17** 40
- [6] Bryan M T, Schrefl T, and Allwood D A 2007 *Appl. Phys. Lett.* **91** 0142502
- [7] Petit D, Jausovec A V, Read D, and Cowburn R P 2008 *J. Appl. Phys.* **103** 114307
- [8] Faulkner C C, Allwood D A, and Cowburn R P 2008 *J. Appl. Phys.* **103** 073914
- [9] Bogart L K, Eastwood D S, and Atkinson D 2008 *J. Appl. Phys.* **104** 033904
- [10] Nam C, Jang Y, Lee K S, and Cho B K 2008 *Nanotechnology* **19** 015703
- [11] Nakatani Y, Thiaville A, and Miltat J 2003 *Nature Mater.* **2** 521
- [12] Porter D G and Donahue M J 2004 *J. Appl. Phys.* **95** 6729
- [13] Bryan M T, Schrefl T, and Allwood D A 2010 *IEEE Trans. Magn.* **46** 1135
- [14] McMichael R D and Donahue M J 1997 *IEEE Trans. Magn.* **33** 4167
- [15] Nakatani Y, Thiaville A, and Miltat J 2005 *J. Magn. Magn. Mater.* **290** 750
- [16] Hayashi M, Thomas L, Rettner C, Moriya R, Jiang X, and Parkin S S P 2006 *Phys. Rev. Lett.* **97** 207205
- [17] Fidler J, Schrefl T, Tsiantos V D, Scholz W, and Suess D 2002 *Comput. Mater. Sci.* **24** 163
- [18] Prejbeanu I L, Buda L D, Ebels U, Viret M, Fermon C, and Ounadjela K 2001 *IEEE Trans. Magn.* **37** 2108
- [19] Kasatani Y, Yamaguchi A, Yamamoto H, and Miyajima H 2010 *Phys. Rev. B* **81** 224425
- [20] Chu Y H, Martin L W, Holcomb M B, Gajek M, Han S J, He Q, Balke N, Yang C H, Lee D, Hu W, Zhan Q, Yang P L, Fraile-Rodriguez A, Scholl A, Wang S X, and Ramesh R 2008 *Nature Mater.* **7** 478
- [21] Dean J S, Bryan M T, Allwood D A, Bance S, Bashir M A, Hrkac G, Goncharov A, and Schrefl T 2009 *IEEE Trans. Magn.* **45** 4067
- [22] Dean J, Bryan M T, Schrefl T, and Allwood D A 2011 *J. Appl. Phys.* **109** 023915

- [23] Cherifi S, Hertel R, Locatelli A, Watanabe Y, Potdevin G, Ballestrazzi A, Balboni M, and Heun S 2007 *Appl. Phys. Lett.* **91** 092502
- [24] Schrefl T 1999 *J. Magn. Magn. Mater.* **207** 66
- [25] Dean J, Bryan M T, Hrkac G, Goncharov A, Freeman C L, Bashir M A, Schrefl T, and Allwood D A 2010 *J. Appl. Phys.* **108** 073903
- [26] Sobolev V L, Chen S C, and Huang H L 1993 *Chin. J. Phys.* **31** 403
- [27] Gentils A, Chapman J N, Xiong G, and Cowburn R P 2005 *J. Appl. Phys.* **98** 053905
- [28] Laufenberg M, Backes D, Buhner W, Bedau D, Klaui M, Rudiger U, Vaz C A F, Bland J A C, Heyderman L J, Nolting F, Cherifi S, Locatelli A, Belkhou R, Heun S, and Bauer E 2006 *Appl. Phys. Lett.* **88** 052507
- [29] Atkinson D, Allwood D A, Xiong G, Cooke M D, Faulkner C C, and Cowburn R P 2003 *Nature Mater.* **2** 85
- [30] Beach G S D, Knutson C, Nistor C, Tsoi M, and Erskine J L 2006 *Phys. Rev. Lett.* **97** 057203
- [31] Hayashi M, Thomas L, Bazaliy Y B, Rettner C, Moriya R, Jiang X, and Parkin S S P 2006 *Phys. Rev. Lett.* **96** 197207
- [32] Hayashi M, Thomas L, Rettner C, Moriya R, and Parkin S S P 2008 *Appl. Phys. Lett.* **92** 112510

### Figure Captions:

Figure 1: The axial magnetization ( $M_x/M_s$ ) profile through the centre of a 150 nm wide, 10 nm thick nanowire containing a transverse wall (TW) or vortex wall (VW) for (a)  $K = 0 \text{ kJ.m}^{-3}$ , (b)  $K = 10 \text{ kJ.m}^{-3}$ ,  $\theta_a = 0 \text{ rad}$  and (c)  $K=10 \text{ kJ.m}^{-3}$ ,  $\theta_a = \pi/2 \text{ rad}$ . The magnetization at  $M_x/M_s = \pm 0.9$ , used to estimate the wall width, is indicated by the horizontal dotted lines. The vertical lines indicate the widths of the TW ( $w_{TW}$ ) and VW ( $w_{VW}$ ) walls when no anisotropy is present. The magnetization structure of transverse (top) and vortex (bottom) walls are shown for each anisotropy condition.

Figure 2: (a) The effective width-to-thickness ratio,  $w'/t'$ , determining the stationary wall width parameter,  $\Delta_{TW}$ , and (b) the analytical Walker breakdown field,  $H_W$ , normalized to the case without anisotropy, in a 100 nm wide, 5 nm thick magnetic wire with various uniaxial anisotropy strengths,  $K$ , and in-plane directions,  $\theta_a$ .

Figure 3: The effect of the in-plane easy axis angle,  $\theta_a$ , on the stationary wall width for up (positive y-magnetization) transverse (TW) and clockwise (CW) and counter-clockwise (CCW) vortex walls (VW) when  $K = 10 \text{ kJ.m}^{-3}$ , normalised to the case when  $K = 0 \text{ kJ.m}^{-3}$ . The analytical model, based on equation 1 with  $\varphi = \pi/2 \text{ rad}$ , predicts the same normalised wall width for transverse and vortex walls.

Figure 4: Micromagnetic ( $\mu\text{mag}$ ) and analytical calculations of the critical widths,  $w_b$ , and thicknesses,  $t_b$ , defining the vortex (VW) and transverse wall (TW) phase boundary with no in-plane anisotropy ( $K = 0 \text{ kJ.m}^{-3}$ ), and with  $K = 10 \text{ kJ.m}^{-3}$ , directed along the wire long axis ( $\theta_a = 0 \text{ rad}$ ) and perpendicular to the wire long axis ( $\theta_a = \pi/2 \text{ rad}$ ).

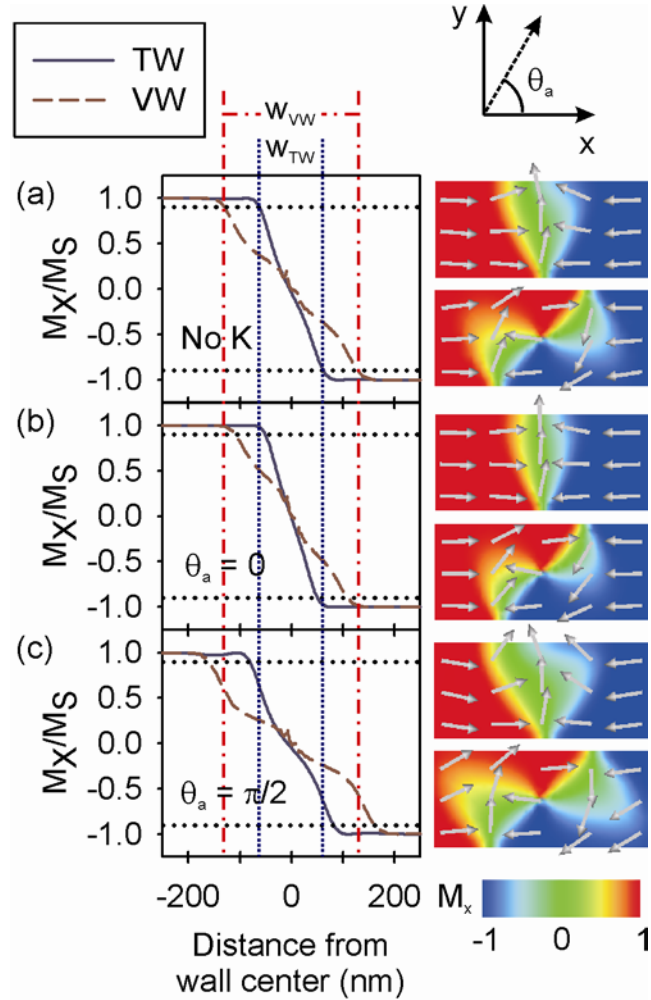


Figure 1: The axial magnetization ( $M_x/M_s$ ) profile through the centre of a 150 nm wide, 10 nm thick nanowire containing a transverse wall (TW) or vortex wall (VW) for (a)  $K = 0 \text{ kJ.m}^{-3}$ , (b)  $K = 10 \text{ kJ.m}^{-3}$ ,  $\theta_a = 0 \text{ rad}$  and (c)  $K=10 \text{ kJ.m}^{-3}$ ,  $\theta_a = \pi/2 \text{ rad}$ . The magnetization at  $M_x/M_s = \pm 0.9$ , used to estimate the wall width, is indicated by the horizontal dotted lines. The vertical lines indicate the widths of the TW ( $w_{TW}$ ) and VW ( $w_{VW}$ ) walls when no anisotropy is present. The magnetization structure of transverse (top) and vortex (bottom) walls are shown for each anisotropy condition.

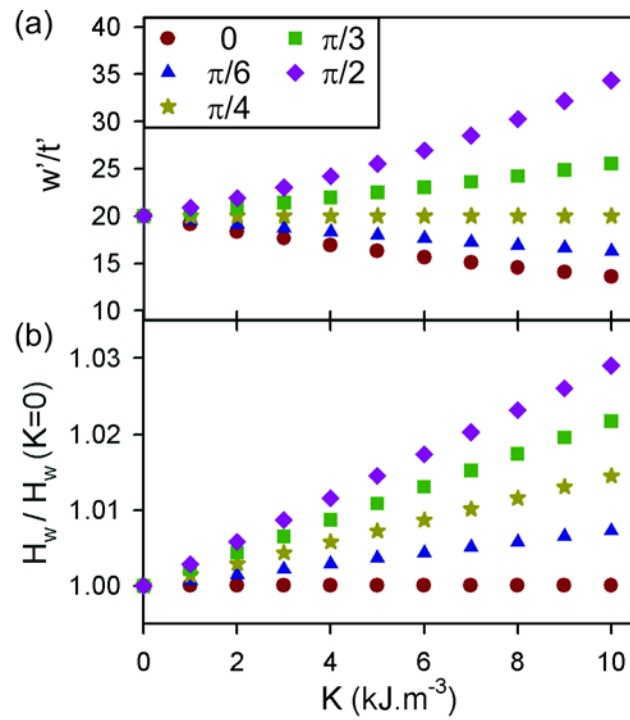


Figure 2: (a) The effective width-to-thickness ratio,  $w'/t'$ , determining the stationary wall width parameter,  $\Delta_{TW}$ , and (b) the analytical Walker breakdown field,  $H_w$ , normalized to the case without anisotropy, in a 100 nm wide, 5 nm thick magnetic wire with various uniaxial anisotropy strengths,  $K$ , and in-plane directions,  $\theta_0$ .

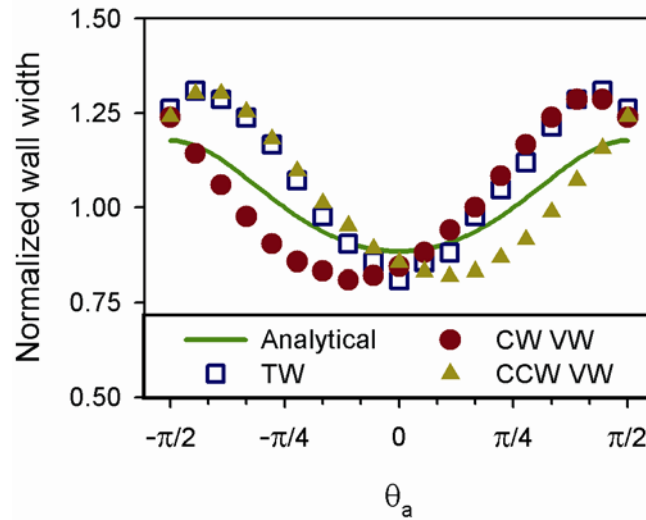


Figure 3: The effect of the in-plane easy axis angle,  $\theta_a$ , on the stationary wall width for up (positive  $y$ -magnetization) transverse (TW) and clockwise (CW) and counter-clockwise (CCW) vortex walls (VW) when  $K = 10 \text{ kJ.m}^{-3}$ , normalised to the case when  $K = 0 \text{ kJ.m}^{-3}$ . The analytical model, based on equation 1 with  $\varphi = \pi/2$  rad, predicts the same normalised wall width for transverse and vortex walls.

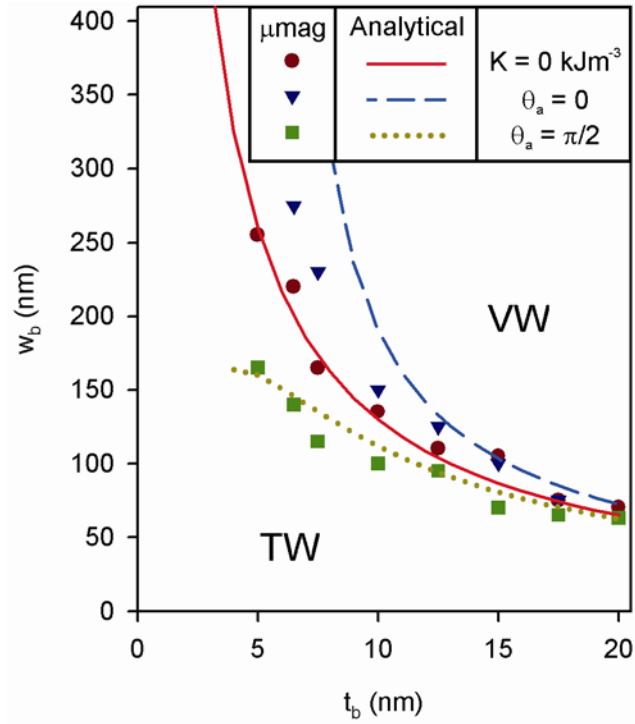


Figure 4: Micromagnetic ( $\mu\text{mag}$ ) and analytical calculations of the critical widths,  $w_b$ , and thicknesses,  $t_b$ , defining the vortex (VW) and transverse wall (TW) phase boundary with no in-plane anisotropy ( $K = 0 \text{ kJ.m}^{-3}$ ), and with  $K = 10 \text{ kJ.m}^{-3}$ , directed along the wire long axis ( $\theta_a = 0 \text{ rad}$ ) and perpendicular to the wire long axis ( $\theta_a = \pi/2 \text{ rad}$ ).